

Electronic Supplementary Material (ESI) for Lab on a Chip

## **Luminometric sub-nanoliter droplet-to-droplet Arrays (LUMDA) and Its Application to Drug Screening by Phase I Metabolism Enzymes**

Giuseppe Arrabito,<sup>a</sup> Clelia Galati,<sup>b</sup> Sabrina Castellano<sup>c</sup> and Bruno Pignataro<sup>d,\*</sup>

<sup>a</sup>Scuola Superiore di Catania, Via Valdisavoia 9, 95123, Catania, Italy; <sup>b</sup>ST Microelectronics, Stradale Primosole, 95121 Catania, Italy; <sup>c</sup>Dipartimento di Scienze Farmaceutiche e Biomediche, Università degli Studi di Salerno, via Ponte don Melillo, 84084, Fisciano (Salerno), Italy; <sup>d</sup>Dipartimento di Chimica “S. Cannizzaro”, Università degli Studi di Palermo, V.le delle Scienze, Parco d’Orleans II, 90128, Palermo, Italy. E-mail: bruno.pignataro@unipa.it

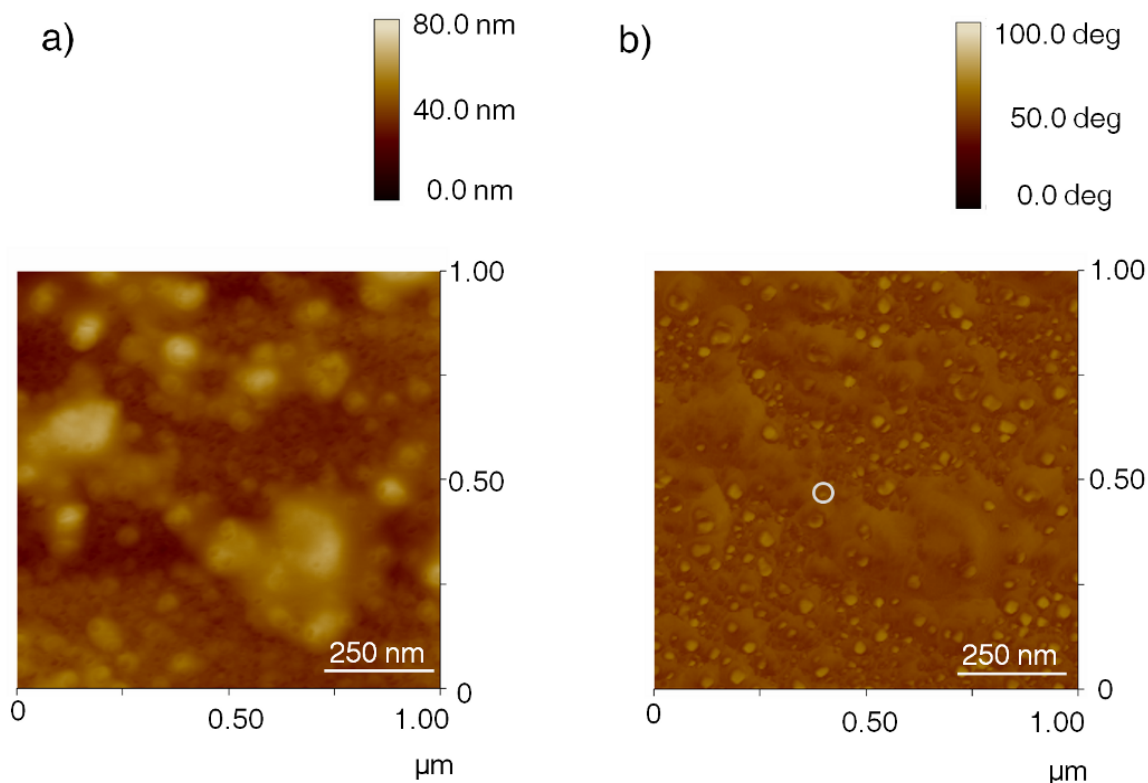
### **Table of Contents**

- **Materials**
- **Methods**
- **Droplets microarray fabrication by inkjet printing**
- **Optimization of Inkjetting process**
- **Effect of mechanical stresses upon CYP3A4 activity**
- **Multi-droplets Microarray Fabrication**
- **Optical Calibration of the Luminometric signal**



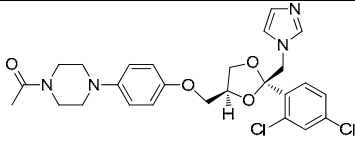
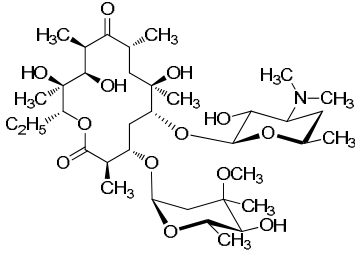
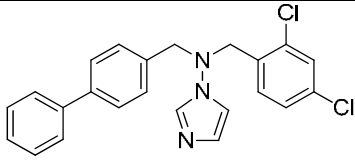
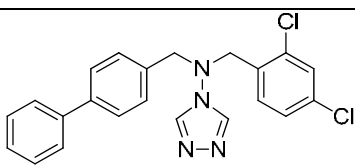
## Materials

CYP3A4 enzyme was purchased from PROMEGA as Screening System containing the Luciferin Detection Reagent (i.e. Luciferase enzyme, Luciferin-IPA, namely 2-[4-[bis(propan-2-yloxy) methyl]-4,5-dihydro-1,3-thiazol-2-yl]-1,3-benzothiazol-6-ol and Luciferase Buffer with Esterase), CYP3A4 liposomes (1pmol/ $\mu$ L) + P450 Reductase, Cytochrome b5, NADPH Regeneration System consisting of Solution A having NADP<sup>+</sup> and glucose-6-phosphate (G6P) supplied as a 20X concentrate and Solution B containing glucose-6-phosphate dehydrogenase. CYP3A4 liposomes are prepared from baculovirus-infected insect cells and co-express human CYP3A4 enzyme, P450 reductase and cytochrome b5. MTMOS (methyltrimethoxysilane, 98%), DMSO (Dimethyl sulfoxide, BioReagent, for molecular biology,  $\geq$  99.9%), acetonitrile anhydrous (99.8%), glycerol (ACS reagent,  $\geq$  99.5%), ketoconazole ( $\geq$  98%; 531,4 g/mol) and erythromycin (BioReagent, suitable for cell culture, 733.93 g/mol) were purchased from Sigma Aldrich. Ultra pure water (Millipore milli-Q, 18.2 M $\Omega$ ·cm) was used for preparation of the ink solutions.



**Figure S1.** Scanning Probe Microscopy characterization of CYP3A4, human P450 reductase and cytochrome b5 proteins immersed in a liposome matrix. (a) and (b) are respectively the height (topography) and phase images. The circle in (b) indicates a proteic spherical object.

Figure S1 reports on SPM investigation of membranes co-expressing CYP3A4, human P450 reductase and cytochrome b5. A 5  $\mu$ L droplet containing CYP3A4 (10 nM) in its own buffer was casted on silicon dioxide surfaces and left dry at room temperature. The phase image shows globular structures of various sizes (3 - 30 nm) likely consisting of aggregates of proteins. Azoles TS51 and TS28 (TableS1) were synthesized following our previously reported route.<sup>1,2</sup>

Compound	Formula	MW
Ketoconazole		531.43
Erythromycin		733.93
TS51		408.32
TS28		409.31

**Table S1.** Compounds employed for Inhibition Assays on CYP3A4 liposomes.

Thermal silicon dioxide (t-SiO<sub>2</sub>) substrates (80 nm thermal oxide thickness) were used as solid supports for the arrays. Silicon based support slides were prepared as follows. After standard cleaning, etching in diluted HF (aq) 1%, and rinsing in deionized water, single crystalline, Czochralski grown, (100) oriented, p type silicon slices were mounted in a furnace operating at atmospheric pressure. Thermal oxidation was performed at a controlled rate in order to reproducibly grow layers of silicon oxide of a defined thickness. The wafers were then cut in pieces by the dimensions of conventional microscope slides (75 x 25 mm). Such oxide thickness act as an antireflection layer which allows reducing, in respect to silicon with native oxide, the optical background (see Figure S2) – a significant benefit for the sensitivity of the luminometric detection approach (Figure S8).

## Methods

**Preparation of solid substrates.** Thermal silicon dioxide (t-SiO<sub>2</sub>) substrates were immersed in acetone (30 min) and washed with millipore water thoroughly. Subsequently, oxygen plasma cleaning was carried out (1 mbar 75 W, 10', March Barrel Plasmod) and finally MTMOS (Methyltrimethoxysilane) was spin-coated (30 μL, 1000 RPM, 30", TP 6000 Dispense and Spinning System, Sulzer Electro Technique) in order to slightly increase surface hydrophobicity (measured water contact angle was 23-25 degrees) and also for facilitating the easy attachment of individual microarray spots and preventing local spreading and merging of spots. Before use, MTMOS-coated slides were stored in the dark at -20 °C. It is known that CYP activity may be inhibited nonspecifically by binding of CYP3A4 membranes and/or substrates to a surface that has been treated for enhancing hydrophobicity. Accordingly, the slight hydrophobicity of such prepared surfaces does not affect the enzymatic activity.<sup>4,5</sup>

**Surface Characterization.** Optical images were obtained by a Nikon Eclipse ME600 Microscope and managed by using the software Lucia G on Mutech v 4.60 (Nikon, Italy). The morphology of the molecular surfaces were inspected by Dynamic scanning force microscopy (SFM) in air using a commercial instrument (Multimode Nanoscope IIIa, Digital Instruments, Santa Barbara, California) equipped with a phase extender apparatus and a Q-box module. Commercially available etched-silicon probes with a pyramidal shaped tip having a nominal curvature of 10 nm and a nominal internal angle of 35° were used. During scanning, the 125- $\mu\text{m}$  long cantilever, with a nominal spring constant in the range 20-100 N/m, oscillated at its resonance frequency ( $\sim 330$  kHz). Height and phase images were collected by capturing 512 x 512 points in each scan, and the scan rate was maintained below 1 line/s. During imaging, temperature and humidity were about 293 K and 40%, respectively.

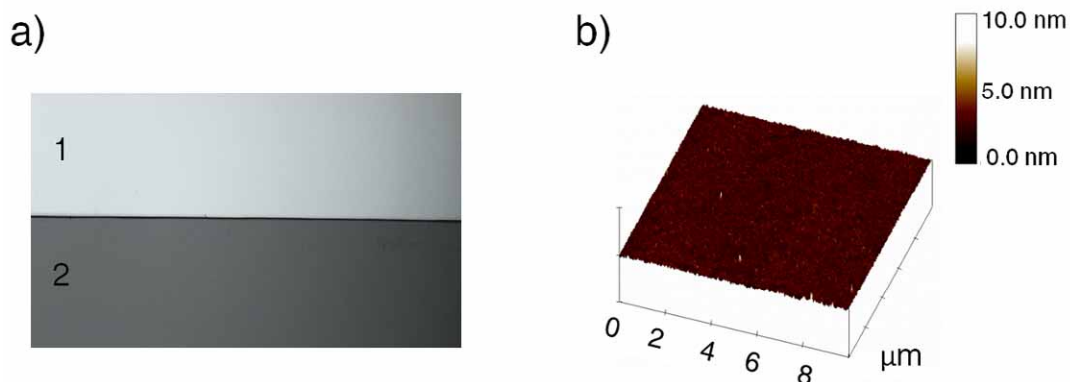


**Figure S2.** Characterization of silicon dioxide surfaces. (a) Optical characterization of native silicon oxide (1), and thermal 80 nm thick  $\text{SiO}_2$  (2). (b) AFM characterization of (2) after the MTMOS treatment.

Figure S2 reports on the characterization of silicon dioxide surfaces employed in the work. In (a), a 5 X optical image showing two different slides with different  $\text{SiO}_2$  thickness in physical contact. Native silicon oxide surface (here defined as native oxide) (1) shows a mean gray value of 177.34 ( $\pm 10.6$ ) to be compared with the mean gray values of t- $\text{SiO}_2$  surface (2) which is 49.3 ( $\pm 6.6$ ). The lower brightness of the t- $\text{SiO}_2$  substrate can be ascribed to the antireflecting silicon oxide layer which reduces the stray light reaching the detector. In (b), an SPM investigation of a MTMOS covered t- $\text{SiO}_2$  surface is reported. Surface roughness (expressed as RMS) as measured on 10  $\mu\text{m}$  scan size is about 0.25 nm.

### Preparation of bio-inks for printing

- **Inhibitors ink.** Ketoconazole was dissolved in acetonitrile to get a 62.7 mM initial solution which was then diluted to get a 1  $\mu\text{M}$  solution (PBS buffer 0.1 M, < 0.1 % acetonitrile, 30% glycerol). Erythromycin, TS51 and TS28 were dissolved in DMSO to get respectively 20 mM, 25 mM, 31 mM solutions which were then diluted in to get a final 20  $\mu\text{M}$  solution (PBS buffer 0.1 M, < 0.1 % DMSO, 30% v/v glycerol). The solutions were mixed, vortexed and then loaded to the cartridge.

- **CYP3A4 ink.** CYP3A4 liposomes preparations were thawed rapidly at 37°C. Upon thawing, they were immediately placed on ice. An aliquot was then rapidly mixed with the buffer solution having the enzymatic substrate (Luciferin-IPA 3 mM in DMSO), glycerol and 1M PBS to get a final solution with CYP3A4 at concentration of 16 nM, Luciferin-IPA 24  $\mu\text{M}$ , PBS 0.1 M and glycerol 30% (v/v). The solution was immediately loaded into the cartridge and used within 24h for the experiments.

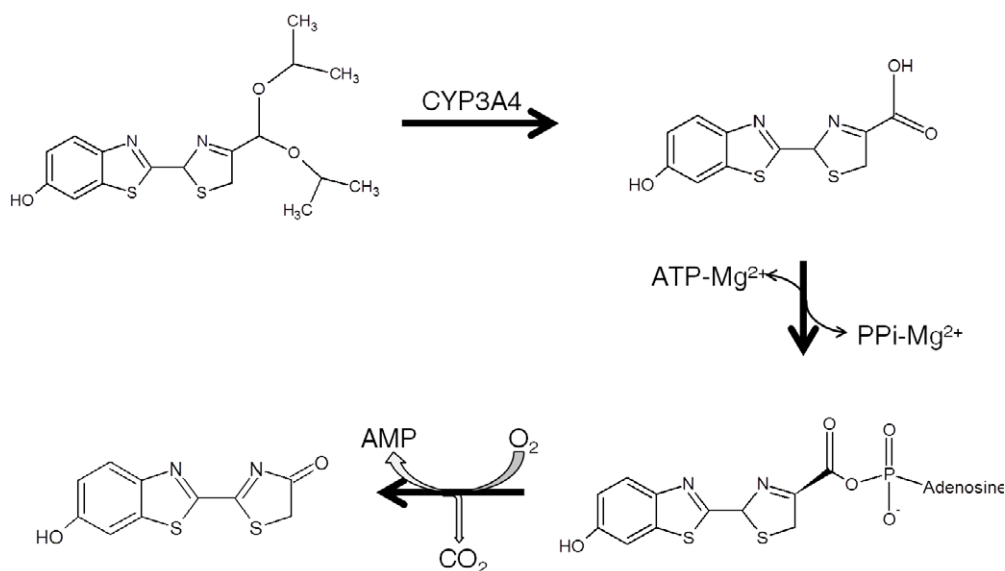
- **Regeneration systems ink.** The two solutions of the NADPH Regeneration System (Solution A and Solution B) were thawed and then put on ice. Then they were rapidly combined together with PBS buffer solution and glycerol in order to get a 8X solution having 0.1 M PBS and 30% v/v glycerol. This solution was mixed and loaded into the cartridge. Upon droplet mixing in the spots, final concentration of the Regeneration System contained 1.3 mM  $\text{NADP}^+$ , 3.3 mM glucose-6-phosphate, 3.3 mM of  $\text{MgCl}_2$  and 0.4 U/ml glucose-6-phosphate dehydrogenase. The NADPH regeneration system is stable for repeated freeze-thaw cycles.

- **Luminometric Detection Reagent ink.** The Luciferin Detection Reagent (lyophilized) and Reconstitution Buffer with esterase were equilibrated to room temperature. The entire contents of the Reconstitution Buffer with esterase was transferred

to the amber bottle containing the lyophilized Luciferin. Mixing was executed by swirling and inverting several times (vortexing has to be avoided since it would lead to foaming due to the presence of the surfactant present in the buffer solution) in order to obtain a homogeneous solution which was added of glycerol (30% v/v), mixed again before loading to the cartridge. The reconstituted Luciferin Detection reagent is stable at room temperature for 24 hours or at 4°C for one week without significant loss of activity.

**- Inkjet Dispensing.** Picoliter Droplets were dispensed on silicon dioxide substrates by using a Dimatix Materials Printer (DMP-2800, Fuji Film) at 40% Relative Humidity and 22-23°C. This instrument was equipped with user fillable piezo-driven inkjet print cartridges, each with 16 nozzles 254  $\mu\text{m}$  spaced and 21.5  $\mu\text{m}$  in diameter. The droplets are emitted at a jetting frequency of 5 kHz with typical flow rates of 10 pL/10  $\mu\text{s}$  (i.e. 1  $\mu\text{L/s}$ ) (considering the times necessary for the formation of a single droplet). The deposited liquids contained all glycerol at 30 % for optimizing drop rheological properties and resolving evaporation issues in droplets. We verified that final liquid spots were stable for more than 8 hours without changing shape and volume (see Fig. S10) allowing for dispensing the five array layers (Fig. S11, 10-15 minutes), incubating (25 minutes) and saturating the kinetics processes (20-30 minutes). Indeed, thanks to the high hygroscopic properties of glycerol, water content in drops remains constant for few hours at 40% relative humidity. At a relative humidity higher than 70%, glycerol moisturizing effects over compete water evaporation increasing the water content of the liquid spots, whereas at values lower than 20% water evaporation is fast leading to a decrease in the spot volume. Microarrays were realized in a 6 x 12 spots format spot-to-spot spacing of 500  $\mu\text{m}$ , thus leading to 72 spots usable for the assay including a reference spot per line (blanket spots) deriving from liposomes without CYP3A4. Spot size was a result of the coalescence of multiple droplets (drop-to-drop pitch of 5  $\mu\text{m}$ ) measuring  $155 \pm 31$   $\mu\text{m}$  in diameter.

**Luminometric CYP3A4 assay.** Scheme S1 reports on the CYP3A4 luminometric assay according to the manufacturer's protocol (PROMEGA). The CYP3A4 catalyzed reaction is performed by incubating a luminogenic CYP substrate with a CYP enzyme and NADPH regeneration system. The luminogenic P450-Glo™ substrates are derivatives of beetle luciferin [(4S)-4,5-dihydro-2-(6-hydroxybenzothiazolyl)-4-thiazolecarboxylic acid or D-luciferin], a substrate of firefly luciferase. Luciferin-IPA is the CYP3A4 substrate chosen for the production of D-luciferin which, in turn, reacts to produce photons with high-efficiency (80%-90%).<sup>6,7</sup> According to the manufacturer's instructions, Luciferin-IPA is among the most sensitive substrate for CYP3A4 screening applications and shows only a modest inhibition by DMSO. CYP3A4 assays are performed in two steps. The first consists in the Cytochrome P450 reaction in which Luciferin-IPA substrate is converted by CYP3A4 to D-luciferin. In the second step, D-luciferin is detected as a luminescent signal from the Luciferase reaction. This step is initiated by adding an equal volume of Luciferin Detection Reagent which is able to stop the CYP reaction and initiating a luminescent signal that is proportional to the amount of D-luciferin produced in step1. The P450-Glo™ Assays use a proprietary luciferase (Ultra-Glo™ Luciferase) to generate a stable "glow-type" luminescent signal with a half-life greater than four hours.



**Scheme S1.** Luminescent cytochrome P450 assay by employing Luciferase enzyme. (a) Luciferin-Isopropyl acetal, namely 2-(4-(diisopropoxymethyl)-4,5-dihydrothiazol-2-yl)benzo[d]thiazol-6-ol is a substrate for CYP3A4 enzyme: the product of the reaction is D-Luciferin. (b) In presence of ATP-Mg<sup>2+</sup> D-luciferin products light upon reaction with oxygen in a reaction catalyzed by Luciferase enzyme.

**Multi-droplets Microarray Fabrication.** A sequential multi-droplets inkjet process was carried out to realize the droplets microarray (Figure S3). Droplets of different biochemicals were printed according the following sequential order:

1. PBS buffer (0.1 M - pH 7.4).
2. Test inhibitor ([erythromycin] = 20 μM, [TS28] = 20 μM, [TS51] = 20 μM, [ketoconazole] = 1 μM in PBS buffer (0.1 M - pH 7.4)) printed by employing 1 pL cartridge.
3. CYP3A4 baculosomes (16 nM) + Luciferin-IPA (24 μM) in PBS buffer (0.1 M - pH 7.4).
4. Regeneration System: 10.4 mM NADP<sup>+</sup>, 26.4 mM Glucose-6-phosphate G6P, 26.4 mM MgCl<sub>2</sub>, 3.2 U/ml Glucose-6-phosphate dehydrogenase G6PDH.
5. Luciferase Detection Reagent.

Droplets of inhibitor molecules (volumes ranging from 0 to 180 pL) were combined with buffer solution droplets (volumes ranging from 180 to 0 pL) in order to generate spots having different concentrations of inhibitor molecules in solution. Then, by printing 30 pL of CYP3A4, incubation between the enzyme and the inhibitor occurred together with substrate Luciferin-IPA for at least 10 minutes. The enzymatic reaction started by adding Regeneration System (30 pL): the reaction occurred in a final volume of 240 pL at room temperature for 15 minutes. Finally, spots were added with Luciferase Detection Reagent (240 pL) in order to start the Bioluminescent Reaction in 480 pL (150 μm diameter) spots (scheme S1).

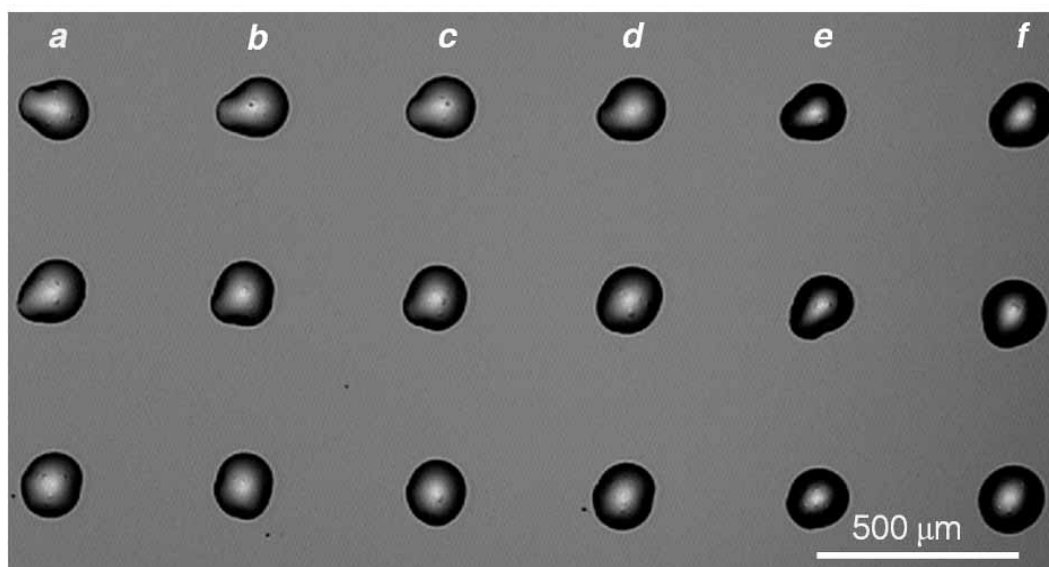


**Figure S3.** Optical image showing an example of a LUMDA chip array made by a replicate of lines with 500 microns pitch. Enzymatic inhibition in spots of columns **b-f** is due to ketoconazole added in the concentrations reported in table S2.

By employing this multidroplets approach, the array shows a gradient in the concentration of model inhibitors of CYP3A4 (Table S2) by varying the volumes (actually the number of droplets) of the printed inhibitor. After 15 minutes of incubation at room temperature, bright field images were captured with a SONY Exwave HAD Color Video Camera Digital mounted on a Nikon Eclipse ME600 optical microscope. The acquisition time for all the images was set-up as 40 ms. Images were then analyzed via MacBiophotonics ImageJ Software.

In between each new biomolecular printing step, since a different cartridge is required for each dispensed biomaterial, MEMS Alignment procedure was executed in order to address droplets on spots printed in the previous printing steps. In order to achieve that, the position of a new cartridge always had to be calibrated with respect to the position of the previous pattern. In this regard, in an area distant from the printing area of concern, a sub-set of the layer of interest was printed. Then by employing DMP-2800 Software, the coordinates of the upper left printed spot (consisting of a spot of 160 pL) of the printed



array was given ( $X = 0, Y = 0$ ) to the software. Then the cursor was placed in the position of this selected upper left spot to allow the software to adjust any positional offset on the plane due to each cartridge. Each different cartridge requires a different alignment procedure and that also depending on the pattern geometry, the alignment error can be different. This procedure only requires 1-2 minutes and is featured with a positional repeatability of 25  $\mu\text{m}$ .

Ink-jetted Layer	a	b	c	d	e	f
Buffer	180 pL	180 pL	170 pL	120 pL	90 pL	0 pL
Inhibitor (C $\mu\text{M}$ )	0 pL	1 pL	10 pL	60 pL	90 pL	180 pL
CYP3A4 + LIPA	30 pL	30 pL	30 pL	30 pL	30 pL	30 pL
G6PDH + G6P	30 pL	30 pL	30 pL	30 pL	30 pL	30 pL
Luciferase + ATP	240 pL	240 pL	240 pL	240 pL	240 pL	240 pL

Spot	[Inhibitor] ( $\mu\text{M}$ )
a	0 C
b	$4.15 \cdot 10^{-3} \text{C}$
c	$4.17 \cdot 10^{-2} \text{C}$
d	$2.50 \cdot 10^{-1} \text{C}$
e	$3.75 \cdot 10^{-1} \text{C}$
f	$7.50 \cdot 10^{-1} \text{C}$

**Table S2.** Generation of a gradient of inhibitor concentration by multi-droplets inkjet printing. The left table shows volumes (in picoliters) of the inkjetted droplets of every different biochemical substance to realize spots (a to f). The right table shows final inhibitor concentration in spots as diluted from the initial concentration (C  $\mu\text{M}$ ) present in the cartridge.

**Cytochrome P450 Inhibitory Potential of Tested Compounds with Recombinant Human CYP3A4.** The potential inhibitory effect of compounds on CYP3A4 was investigated by Reaction Biology Corp. (RBC) using Vivid® CYP3A4 Red (P2856) from Invitrogen which consists of a Vivid BOMR substrate, a CYP3A4 BACULOSOMES® reagent and a NADPH-regeneration system. Reactions were carried out as suggested from manufacturer provider in a 384-well plate format. Compounds were dissolved in DMSO and tested in 10 doses with 3-fold serial dilutions starting from 300  $\mu\text{M}$  (for Erythromycin and compound TS51, TS28, TS28B) or from 10  $\mu\text{M}$  (for Ketoconazole). All compounds dilutions were pre-incubated at room temperature for 20 min with CYP3A4 enzyme before starting reactions by adding substrate and NADP<sup>+</sup>. Fluorescence was monitored over time in a kinetic assay mode (interval reading every 10 min) for half hour using Ex/Em: 530nm/605nm. The percentages of inhibition were calculated from fluorescence data and analyzed using non-linear regression curve fit with software of Graphpad Prism to calculate the below reported IC<sub>50</sub> values (Table S3).

Compound	Ketoconazole	Erythromycin	TS51	TS28
IC <sub>50</sub> (solution-based assay)	0.0613 $\mu\text{M}$	4.80 $\mu\text{M}$	0.0968 $\mu\text{M}$	6.73 $\mu\text{M}$

**Table S3.** IC<sub>50</sub> inhibition data for Solution-assays on CYP3A4 liposomes.

### Droplets microarray fabrication by inkjet printing

**Set-up of the multi-layered spot arrays fabrication platform: Droplet formation.** As mentioned in the text, stroboscopic images allow an easy interpretation/optimization of the experimental features governing the droplet formation. The fundamental parameters involved are the waveforms, jetting voltage and droplet dynamics. In all the experiments we employed the waveform depicted in Figure S4a with 11.52  $\mu\text{s}$  as a pulse length in both 1 pL and 10 pL cartridges. Thus the fluid flow was in order of 1 microliter per second which is comparable to aerosol dispensing.<sup>8</sup> Importantly, employment of higher pulse lengths (as for instance 23.04  $\mu\text{s}$ ) can significantly reduce biological activity of a printed biomolecule as we previously showed with Glucose Oxidase.<sup>9</sup> Jetting voltage causes strong effects in the droplet shape and in the droplet velocity. Low voltages (i.e. 10-20 V) determine liquid threads shorter than 200  $\mu\text{m}$  while pinching off at the nozzle. After the formation, the droplet tends to maintain a spherical shape with occasional satellite droplets that coalesced with the bigger droplet before reaching the substrate. When the voltages are kept in the higher regime (i.e. 10 - 20 V), the liquid thread at the nozzle exit tends to increase significantly reaching 500  $\mu\text{m}$  at 40 V (Figure S4b). This causes severe stretching stress to the

liquid the leads to break up in several locations of the droplet so forming numerous satellites that can only partially coalesce with the main droplet. The general condition for satellite-free spot was typically produced when the principal droplet and the satellites droplets recombined. This happened when  $av_{ca} \sim v_r > v_s > v_p$  where  $v_a$ ,  $v_r$ ,  $v_s$ ,  $v_p$  are respectively the capillary speed  $v_{ca} = (\gamma/\rho R_{noz})^{1/2}$ , the recoil speed (i.e the rapidity of droplet recoiling under the action of the surface tension), the satellite speed, the primary drop speed.<sup>10</sup> Importantly, droplet velocity after the pinching-off at the nozzle was always kept higher than 5-6 m/s in order to permit the consistent and reproducible formation of well directioned drops with few unwanted satellites. In contrast, droplet speeds higher than 15 m/s typically resulted with long tails and higher number of satellites that finally tend to be difficult to control, whereas at lower speeds, droplets could not be ejected. These findings are in accordance with the results from Feng et al. (ref. 11).

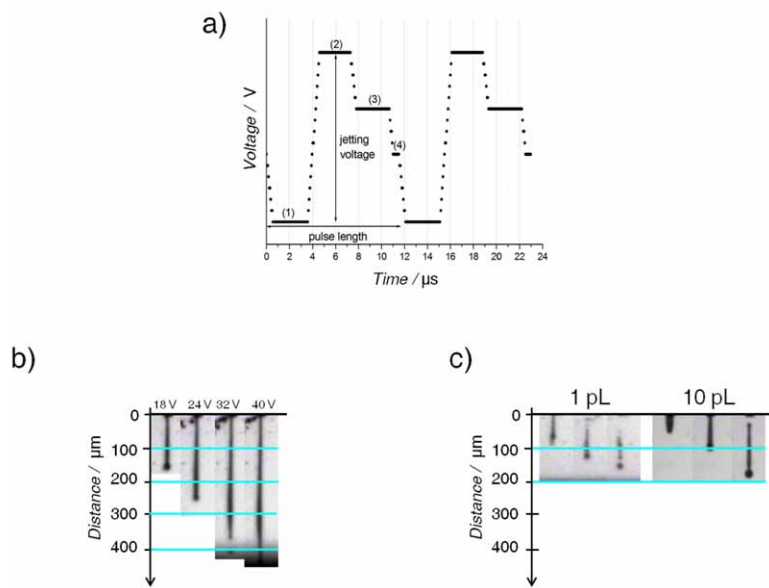


**Figure S4.** (a) Four-segments driving waveform, with single pulse length of 11.52  $\mu$ s. (b) Stroboscopic images showing 10 pL droplets of CYP3A4 pinching-off at the nozzle exit at increasing voltages (18 V, 24 V, 32 V, 40 V). By increasing Jetting voltage, liquid thread length increases. (c) Stroboscopic images showing a 1 pL droplet of ketoconazole and of a 10 pL droplet of 0.1 M PBS buffer pinching off at the nozzle. The voltage for the inkjet printing operation is 12 V.

Importantly, CYP3A4 dispensing by inkjet printing 10 pL droplets (see Figure S4b) required jetting voltages higher than 16-18 V in order to get good droplet directionality and reproducibility (droplet speed higher than 5 m/s). At voltages lower than 18 V, CYP3A4 could not be successfully printed possibly because of issues with clogging at the microchannels. For this reason a Jetting Voltage of 18 V was chosen as an optimal condition since it permitted sufficient ballistic accuracy of the droplet and at the same time does not create satellites due to multiple-breakups. Other bioinks here employed manifested less issues at voltages lower than 18V. Differences were observed to arise when printing 1 pL droplets (i.e. CYP3A4 inhibitors dispensing) if compared to 10 pL droplets. Figure S4c shows a comparison of 1 pL and 10 pL droplets printed at the same voltage (i.e. 12 V) pinching-off at the nozzle. After the pinch-off at the nozzle, multiple breakups due to capillary waves are present for the 1 pL droplet due to its higher speed (about 10 m/s) with respect to the 10 pL droplet (about 5 m/s). However, by employing lower printing voltages, such as 9–10 V, spherical droplets merged without causing satellites.

**Set-up of the multi-layered spot arrays fabrication platform: Droplet impact.** In the fabrication of a multiple droplets microarray, the crucial parameter affecting the final spot resolution is the droplet velocity at the moment of impact. Depending on this value, three different situations can arise. At low impact velocities ( $10^{-2}$ -1 m/s) almost no rim is visible at the impact site, and the droplet is simply deposited on a liquid spot without the formations of rims. At velocities of the order of 1-30 m/s, the motion initiated by the drop is virtually unconstrained and capable of pushing apart a significant liquid mass under the impact site (condition of droplet spreading): the droplet takes the shape of lamellae with a visible outer rim. At higher impact velocities (condition of droplet splashing), the lamellae take the shape of crowns consisting of a thin liquid sheet with an unstable free rim at the top, from which numerous small secondary droplets are ejected. Multi-droplets fabrication was always performed under droplet velocity higher than 5-6 m/s but lower than 30 m/s at voltages around 18-20



V. These conditions permitted to achieve liquid coalescence in the droplets with a certain liquid mass movement under the impact site (i.e. condition of droplet spreading) but without the formation of unwanted liquid crowns consisting of a thin sheet having unstable free rims at the top, from which numerous small secondary droplets would be ejected.<sup>12</sup>

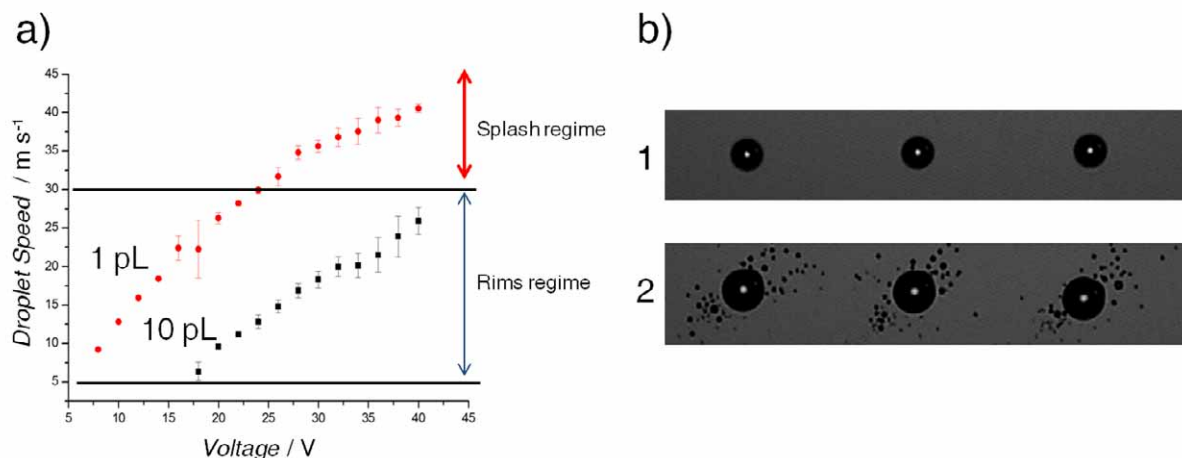


**Figure S5.** In (a) droplet velocity measurements are shown for 1 pL droplet (red dots) and 10 pL droplet (black squares). In (b), optical images of spots consisting of the coalescence of 0.07 M PBS buffer layer (droplet speed of 10 m/s) and a ketoconazole inhibitor layer printed at a droplet speed of 10 m/s (1) or 40 m/s (2).

Figure S5a reports on droplet velocity measured while exiting from the nozzles for 10 pL and 1 pL droplets. Since the effect of surface tension dominates over gravity force at the microscale, velocity of droplet pinching-off from the nozzle can be considered as similar to the velocity at the impact stage. For both 10 pL and 1 pL droplets, speed linearly goes with jetting voltage. However, the speed range for 10 pL droplets is the range 5-25 m/s, while for 1 pL droplet ejecting, the range goes from 9 to 40 m/s (Figure S5a). Interestingly, inkjetting 1 pL droplets of inhibitor at 10 V (Figure S5b1) or at 40 V (Figure S5b2) on a droplet of PBS buffer (volume of about 100 pL) leads to two different final droplets. In the first case, no satellites are formed due to liquid impact, in the second case, several satellites are generated due to the splash.

**Effect of mechanical stresses upon CYP3A4 activity.** Inkjet printing can cause a severe and complex fluid flow phenomenon during droplet generation forming an elongated fluid tail, as observed by stroboscopic images. Due to the piezoelectric pressure, the protein is subjected to both compressive and shear stresses. While the first effect consists in the piezo-induced compression of a biomolecular structure, the second is here briefly explained. During ejection, the fluid is forced from the reservoir through the nozzle, thus experiencing significant velocity gradients. Indeed, close to the orifice walls the fluid flow is significantly slower than that in proximity to the orifice center. This fact leads to a significant shear flow,<sup>13</sup> which in turn may result in a shear strain. In this regard, we already showed how Glucose Oxidase can be deactivated by inkjet printing process, retrieving a prominent role due to the jetting voltage: by increasing jetting voltage from 12 V to 40 V, enzymatic activity is reduced of almost 80%.<sup>9</sup> Also, at the moment of droplet impact on solid surfaces though geometrically different deformations occur. It is thus possible that the involved fluid flows might determine significant damages to complex biomolecular structures during the printing process.<sup>14,15</sup>

In order to verify if the printing process could eventually affect CYP3A4 activity, LUMDA-chips were fabricated with spots in which CYP3A4 layer was printed at different voltages (18 V, 24 V, 32 V, 40V) without enzymatic inhibitors (Figure S6a). After the completion of the multidroplets chip, the optical brightness of the final spots was found to dramatically decrease (mean gray values going from 66.2 at 18 V to 26.0 at 40 V) so confirming that the mechanical stresses connected to droplet formation at the nozzle exit together with the droplet impact on liquid phase can have profoundly affected CYP3A4 structural integrity and function. Moreover, the experiments of enzymatic inhibition via ketoconazole on such less active CYP3A4 liposomes lead to lower Z-factor values being 0.63 for CYP3A4 printed at 18 V, 0.51 V for 24 V, 0.17 for 32 V and reaching -0.71 if CYP3A4 baculosomes were printed at 40 V (Figure S6b). This means that the extracted data from chips lose much of their usefulness if higher CYP3A4 droplet ejection voltages higher than 24 V are employed. Z-factor values were calculated on seven positive control spots (CYP3A4 spots without inhibition) and on seven negative control spots (CYP3A4 spots inhibited with ketoconazole 0.75  $\mu$ M). Also note that AFM images (Figure S1) show globular proteins embedded in a lipidic

membrane. This verifies that the eventual mechanical stress has to be propagated through the lipidic system to proteins (note that baculosomes contain CYP3A4, human P450 reductase) since it consists in a material with viscosities two-three orders of magnitude higher than typical biological liquids.

Many studies have shown that physical properties of the lipids, such as thickness stiffness and curvature can affect the biological function of embedded proteins interacting with their transmembrane domains.<sup>16</sup> In principle, any mechanical stress applied on a membrane should be able to affect the function of any membrane protein. Cells are provided with proteic channels that work as mechano-sensors producing a biochemical signal due to membrane mechanical stress.<sup>17</sup> For example, the dimerization kinetics of the channel-forming peptide gramicidin A can be guided by an externally applied mechanical stress on the membrane, resulting in membrane thinning and decreasing the hydrophobic mismatch between membrane and the gramicidin dimer.<sup>18</sup> Gudi et al. even demonstrated that phospholipid bilayer can even mediate shear stress-induced activation of membrane bound G proteins in absence of protein receptors. By modulating lipidic packing by inserting molecules able to raise the fluidity (i.e. benzyl alcohol) it is possible to increase GTP-ase activity.<sup>19</sup>

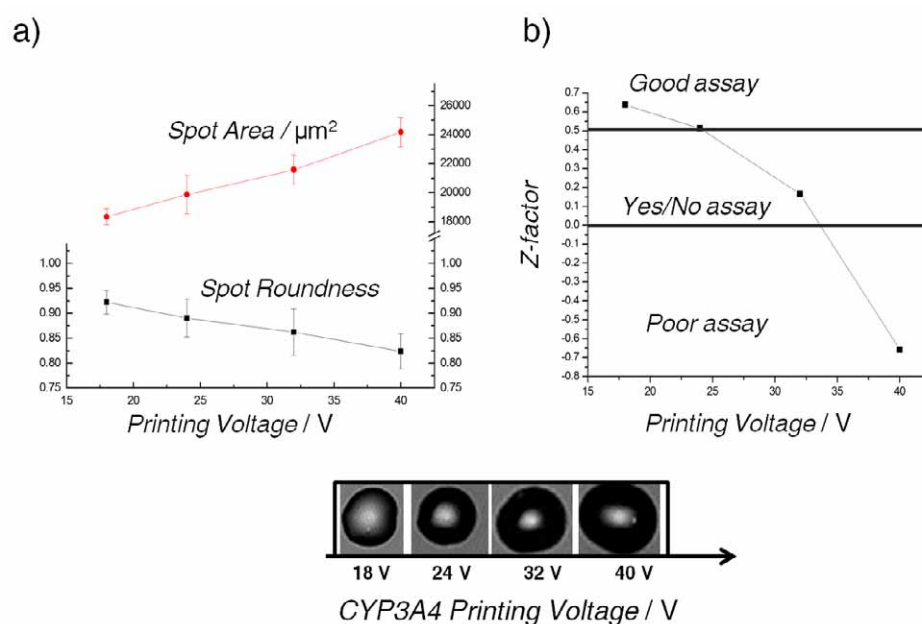


**Figure S6.** Effect of printing voltage on CYP3A4 enzymatic activity on LUMDA-chip. (a) Spot area ( $\mu\text{m}^2$ ) and roundness as a function of CYP3A4 layer Printing voltage. The points are the average values of at least seven different spots. The inset shows LUMDA-chip spots after CYP3A4 printed at different voltages. (b) Z-factor versus CYP3A4 Printing Voltage. CYP3A4 inhibition by erythromycin in the concentration range between  $0.083 \mu\text{M}$  and  $15 \mu\text{M}$ . The points are the average values of at least three different experiments.

### Optical Calibration of the Luminometric signal

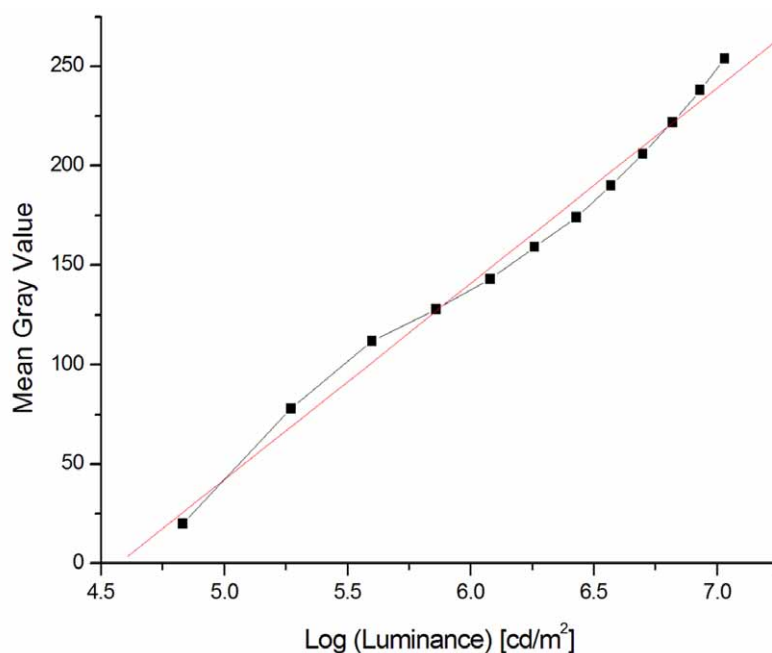


**Figure S7.** Determination of OECF function for the CCD camera employed in the experiments according to the ISO-14524 Digital Camera Contrast Chart – 160:1.

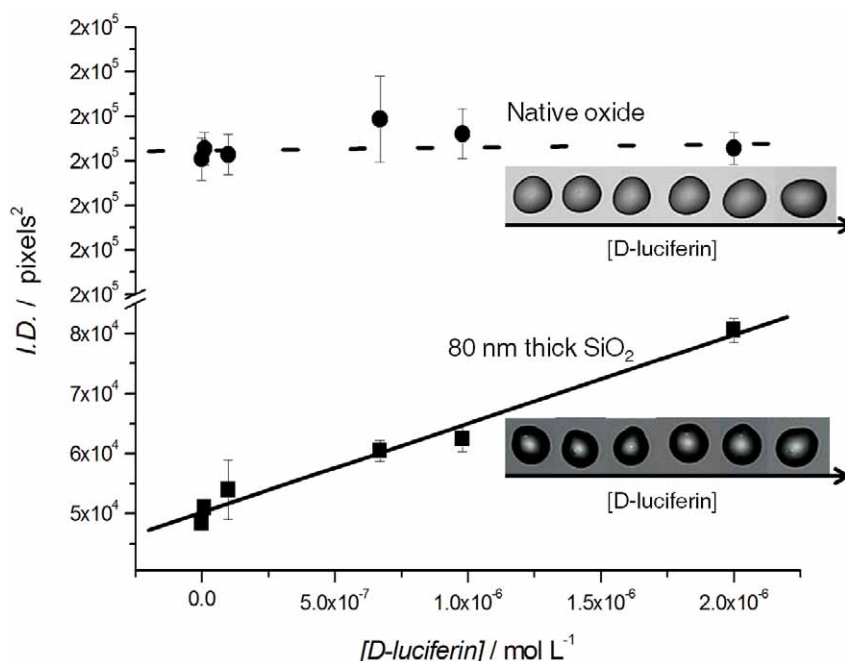
Figure S7 reports on the determination of the Opto-electronic Conversion Function (OECF) of the SONY Exwave HAD Color Video Camera via the employment of the ISO-14524 Digital Camera Contrast Chart – 160:1. The chart uses twelve gray scale patches in visual density increments in conformance to ISO-14524:1999(E) normal contrast ratio (160:1 average scene luminance). The input luminance of the light source is approximately 200 cd on a surface of  $20 \cdot 10^{-6} \text{ m}^2$  in the 5X illumination stage. This means that the incoming Luminance is  $10^7 \text{ cd} \cdot \text{m}^{-2}$ . From the values of optical density reported in the ISO-14524 Digital Camera Contrast Chart – 160:1 for each gray scale patch, it is possible to calculate the outgoing Luminance and correlate its logarithm with the mean gray values of each of the gray patches measured with the camera. The result of these operation leads to the OECF (linear fit  $R^2 = 0.99392$ ), which permits to correlate logarithm of Luminance to Optical Values that can be extracted with the digital camera.

Ink-jetted Layer	a	b	c	d	e	f
Buffer	180 pL	180 pL	170 pL	120 pL	90 pL	0 pL
D-Luciferin (2.6 $\mu\text{M}$ )	0 pL	1 pL	10 pL	60 pL	90 pL	180 pL
CYP3A4 + LIPA	30 pL	30 pL	30 pL	30 pL	30 pL	30 pL
G6PDH + G6P	30 pL	30 pL	30 pL	30 pL	30 pL	30 pL
Luciferase + ATP	240 pL	240 pL	240 pL	240 pL	240 pL	240 pL

Spot	[D-Luciferin] ( $\mu\text{M}$ )
a	0
b	$10^{-2}$
c	$10^{-1}$
d	$6.7 \cdot 10^{-1}$
e	$9.8 \cdot 10^{-1}$
f	2.0

**Table S4.** Generation of a gradient of D-Luciferin concentration by droplets-to-droplets inkjet printing.



**Figure S8.** Optical calibration of D-Luciferin dependent luminescence via CCD-camera on native oxide and 80 nm thick SiO<sub>2</sub> surfaces.

Following manufacturer's protocol (PROMEGA), it is possible to determine the concentration of D-luciferin generated by CYP3A4 enzymatic reactions by comparing the luminescence from enzymatic spots to a D-luciferin standard curve generated via multidroplets inkjet printing. Indeed, a multidroplets microarray can be generated according to the protocol employed in this work in order to generate a gradient of D-luciferin concentration (0.01  $\mu\text{M}$  – 2  $\mu\text{M}$ ) in 240 pL spots (Spots **a-d** Table S4) on native oxide or on t-SiO<sub>2</sub>. Finally, these spots were added with Luciferase Detection Reagent (240 pL) in order to start the Bioluminescent Reaction in 480 pL spots. Results are expressed as Integrated Density (I.D.) a function of D-luciferin concentration (expressed in  $\mu\text{M}$ ). Importantly, the SiO<sub>2</sub> thickness greatly affects the optical output (Figure S8). In the case of native oxide surfaces, integrated density lies on  $1.9 \cdot 10^5$  and does not vary as a function of D-luciferin concentration, while on t-SiO<sub>2</sub> surfaces, integrated density linearly goes with D-Luciferin concentration in the range of  $5 \cdot 10^4$  -  $8 \cdot 10^4$ . This different behavior can be ascribed to the different specific brightness of the two surfaces as emerged from the optical analysis. Hence, the luminance signal coming from the spots on native oxide surfaces is higher than that from t-SiO<sub>2</sub>. However in the case of native oxide, the signal is mainly due to the photons transmitted from the surface and does not depend on the concentration of D-Luciferin in the spots. Then, the luminometric assay in droplets would lose all its sensitivity. For this reason, it is necessary to employ t-SiO<sub>2</sub> surfaces (e.g. 80 nm thickness) for LUMDA chip applications. Importantly, the limit of detection (the average value of Integrated Density of the control plus two times its standard deviation<sup>20</sup>) results about 10 nM. Such value is one order of magnitude higher than the typical sensitivity obtained by luminometric devices, although by using Peltier-cooled cameras, sensitivity can be dramatically increased.<sup>21</sup> The linear response here ranges by two-orders of magnitude in D-luciferin concentration. Moreover, the integrated density value from all our experiments was never higher than the 2  $\mu\text{M}$  standard.

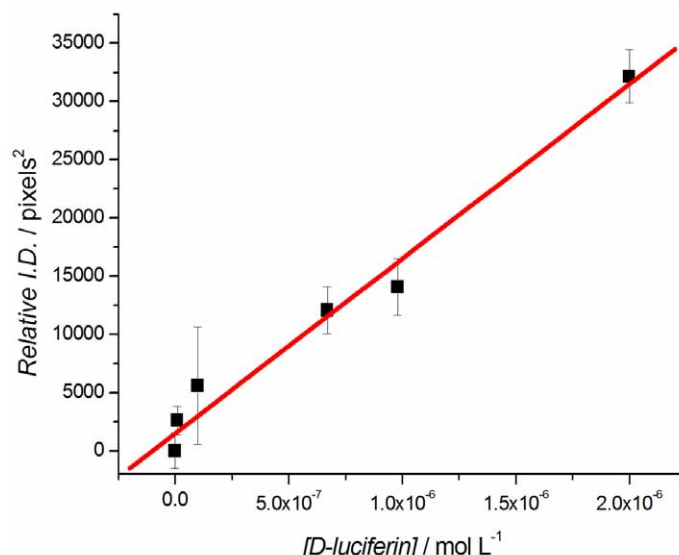


**Figure S9.** Optical calibration of D-Luciferin dependent luminescence, expressed as Relative Integrated Density (i.e. the relative integrated densities values calculated by subtracting optical integrated density value of the spot without D-luciferin from the integrated density values of the spots containing increasing concentrations of D-luciferin).

**CYP3A4 kinetics in droplets.** From the linear fitting of the curve ( $R^2 = 0.9917$ ) showing Relative I.D. versus D-luciferin concentration (Figure S9) it is possible to correlate the moles of D-luciferin produced from the CYP3A4 catalyzed reaction in 240 pL droplets and the integrated density.

The relation is:  $Moles\ of\ D-luciferin = 1.50 \cdot 10^{-20} \cdot [Relative\ I.D.]$

(where *Relative I.D.* stands for relative integrated densities values calculated by subtracting optical integrated density value of the spot without D-luciferin from the I.D. values of the spots containing increasing concentrations of D-luciferin).

Following manufacturer's protocol (PROMEGA) and adapting it to LUMDA chip, CYP3A4 reaction rate can then be calculated as the amount of atto-moles of D-luciferin produced in one spot of 240 pL in 15 minutes of reaction at R.T. with 0.5 attomoles of CYP3A4 (the amount of CYP3A4 present in one spot of 240 picoliters being CYP3A4 concentration in the spot equal to 2 nM). From this definition, reaction rate can be correlated to Relative I.D. in order to measure CYP3A4 activity in droplets (expressed as atto moles of D-luciferin/atto mole of CYP3A4/minute) from the *Relative I.D.* :

$CYP3A4\ activity\ [attomole\ D-luciferin/attomole\ CYP3A4/minute] = 2.04 \cdot 10^3 \cdot Relative\ (I.D.)$

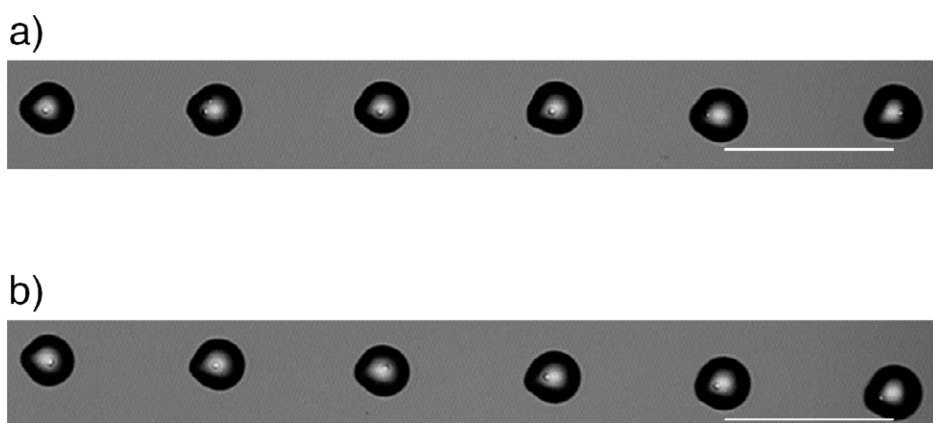


**Figure S10.** Optical images of LUMDA-chip lines a) after assay completion under the described procedures and b) after ~8 hours at room temperature. No significant change in spot morphology is evident (scale bar 500  $\mu$ m).

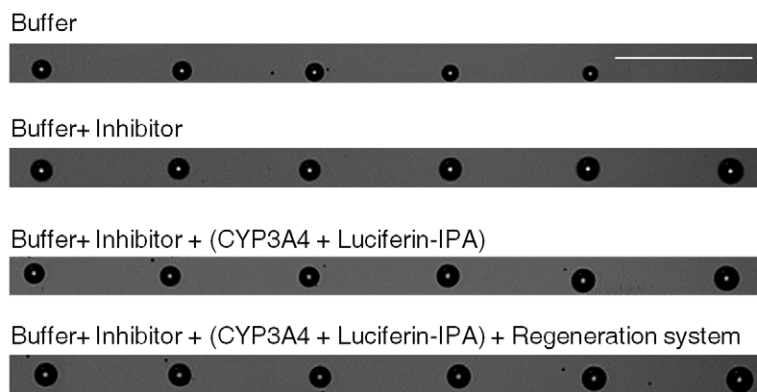


**Figure S11.** Optical images showing sequential droplet-to-droplet print of the first four layers (Buffer, Inhibitor, CYP4A liposomes +Luciferin-IPA, Regeneration System) of a LUMDA-chip at different stages of formation. In the time-scales for droplet-to-droplet spots fabrication (10-15 minutes), evaporation issues can be totally neglected also if several different spotting volumes are used within layers (scale bar 500  $\mu\text{m}$ ).

## References

1. S. Castellano, G. Stefancich, C. Musiu and P. La Colla, *Arch. Pharm. Pharm. Med. Chem.* **2000**, 333, 299–304.
2. S. Castellano, G. Stefancich, R. Ragno, K. Schewe, M. Santoriello, A. Caroli, R. W. Hartmann and G. Sbardella, *Bioorg. Med. Chem.* **2008**, 16, 8349–8358.
3. M. Cretich, G. di Carlo, R. Longhi, C. Gotti, N. Spinella, S. Coffa, C. Galati, L. Renna, M. Chiari, *Anal. Chem.* **2009**, 81, 5197–5203.
4. S.M. Sukumaran, B. Potsais, M.-Y. Lee, D.S.Clark, J.S. Dordick, *J. Biomol. Screen.* **2009**, 14, 668-678.
5. M.-Y. Lee, C.B. Park, J.S. Dordick, D.S. Clark, *Proc. Natl. Acad. Sci. USA* **2005**, 102, 983-987.
6. H.H. Seliger, W.D. McElroy, *Biochem. Biophys. Res. Commun.* **1959**, 1, 21–24.
7. H.H. Seliger, W.D. McElroy, *Arch. Biochem. Biophys.* **1960**, 88, 136–141.
8. D.N. Gosalia, S.L. Diamond, *Proc. Natl. Acad. Sci. USA* **2003**, 100, 8721–8726.
9. G. Arrabito, C. Musumeci, V. Aiello, S. Libertino, G. Compagnini, B. Pignataro, *Langmuir* **2009**, 25, 6312-6318.
10. H. Dong and W. W. Carr, J. F. Morris, *Phys. Fluids* **2006**, 18, 072102.
11. J. Q. Feng, *J. Imaging Sci. Technol.* **2002**, 46, 398–408.
12. A.L. Yarin, *Annu. Rev. Fluid Mech.* **2006**, 38, 159–92.
13. B.R. Ringeisen, C.M. Othon, J.A. Barron, D. Young, B.J. Spargo, *Biotechnol. J.* **2006**, 1, 930–948.
14. C.C. Cook, T. Wang and B. Derby, *Chem. Commun.* **2010**, 46, 5452–5454.
15. G.M. Nishioka, A.A. Markey, C. K. Holloway, *J. Am.Chem. Soc.* **2004**, 126, 16320–16321.
16. R. Phillips, T. Ursell, P. Wiggins, P. Sens, *Nature* **2009**, 459, 379-385.
17. O.S. Andersen, R.E. Koeppe, *Annu. Rev. Biophys. Biomol. Struct.* **2007**, 36,107–130.
18. M. Goulian, O.N. Mesquita, D.K. Fygenson, C. Nielsen, O.S. Andersen, A. Libchaber, *Biophys. J.* **1998**, 74, 328–337.
19. S. Gudi, J.P. Nolan, J.A. Frangos, *Proc. Natl. Acad. Sci. USA* **1998**, 95, 2515-2519.



20. Harris D. C. in *Quantitative Chemical Analysis*, 4th ed.; W. H. Freeman and Co.: New York, **1995**.
21. K. Salama, H. Eltoukhy, A. Hassibi, A. El Gamal, *Biosens. And Bioelectr.*, **2004**, 19, 1377-1386.